ACS OMEGA

Open Access

http://pubs.acs.org/journal/acsodf

Article

Synthesis and Spectroscopic Characterization of Schiff Base Metal Complexes, Biological Activity, and Molecular Docking Studies

Ganesan Venkatesh,* Palanisamy Vennila, Savas Kaya,* Samia Ben Ahmed, Paramasivam Sumathi, Vadivel Siva, Premkumar Rajendran, and Chennapan Kamal

Cite This: *ACS Omega* 2024, 9, 8123−8138

Read Online

ACCESS | Metrics & More | Article Recommendations | Supporting Information

ABSTRACT: New cobalt(II), copper(II), and zinc(II) Schiff metal complexes were synthesized by the condensation reaction of 4-nitrobenzene-1,2-diamine with 3−4-(diethylamino)-2-hydroxybenzaldehyde. Fourier transform infrared, nuclear magnetic resonance, ultraviolet−visible, electron paramagnetic resonance, and high-resolution electrospray ionization mass spectrometry and powder X-ray diffraction were used to characterize the synthesized H_2L and its metal complexes. Conductance measurements, magnetic moment estimation, and metal estimation have all been determined and discussed. The electrochemical properties of the synthesized compounds have been determined and discussed using cyclic voltammetry. The molecular structures of H_2L and its metal complexes have been optimized using the B3LYP functional and the 6-31G (d,p) basis set, and their parameters have been discussed. The quantum chemical properties of these synthesized compounds have been predicted through charge distribution and molecular orbital analysis. The biological properties of the synthesized compounds' antioxidant, antifungal, and antibacterial activity have been studied and discussed. Furthermore, H_2L and its complexes have been docked with HER2-associated target proteins in breast cancer.

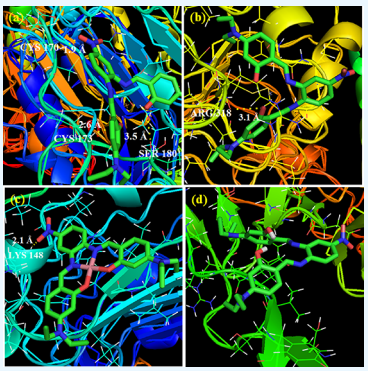

1.0. INTRODUCTION

In recent years, there has been notable attention among academic researchers on Schiff base ligands due to their diverse structural characteristics and wide range of physicochemical properties. This has led to the exploration of various applications for these ligands.[1−4] The interest in Schiff base stems from their structural versatility, which allows them to be effectively employed as asymmetric and stabilizing agents for various complexes in different oxidation states.[3−6] Additionally, Schiff bases play a crucial role in regulating the performance of metals in a wide range of valuable conversions. The coordination of tetradentate Schiff base complexes occurs through dinitrogen and dioxygen donor atoms and results in stable complexes. A few azo-azomethine metal complexes have been used extensively in technology due to their photophysical and energy-transfer capabilities. Because of their stability, electroactivity, thermochromism, and photochromism, Schiff base compounds make excellent intermediates for a variety of uses.[7−10] Numerous reviews revealed that the metallo-organic chemistry of such compounds significantly affected how they acted biologically, highlighting the role played by metals as catalysts in a variety of biological processes.[11−18] Higher electronegative atoms' connected bonding orbitals and electrons can be adsorbed on metal surfaces due to their electrons' C=N faction planarity. This substance contributes significantly to the development of inorganic biochemistry and is used as a substrate in ring closure, cycloaddition, and replacement reactions to produce a variety of biologically active compounds.[19−21]

Some substituted pyridine Schiff bases made from salicylaldehyde were reported by Chohan et al. and demonstrated strong antibacterial activity.[21] Ghosh and co-researchers studied mononuclear Schiff base metal complexes and the results showed an improvement in overall semiconductor and photocatalytic activity.[22] Elemike et al. reported the corrosion activities of three Schiff base compounds based on aniline derivatives. The results indicated that the Schiff base metal complexes act as good inhibitors to prevent corrosion in mild steel.[23] Kargar and co-workers synthesized tetradentate Schiff base ligands and metal complexes with methoxy-salicylaldehyde and substituted phenylenediamine, and the data indicate that the complexes own admirable catalytic activity.[6] The remarkable potency and simplicity of the synthesis of the Schiff base compound's azomethine functional group have contributed significantly to its increased utility today. An active carbonyl group and a primary amine undergo a temperature-controlled catalytic condensation reaction to

Received: October 28, 2023
Revised: January 26, 2024
Accepted: January 31, 2024
Published: February 9, 2024

https://doi.org/10.1021/acsomega.3c08526
ACS Omega 2024, 9, 8123−8138

Scheme 1. Synthetic Route for H_2L, Co(II), Cu(II), and Zn(II) Complexes

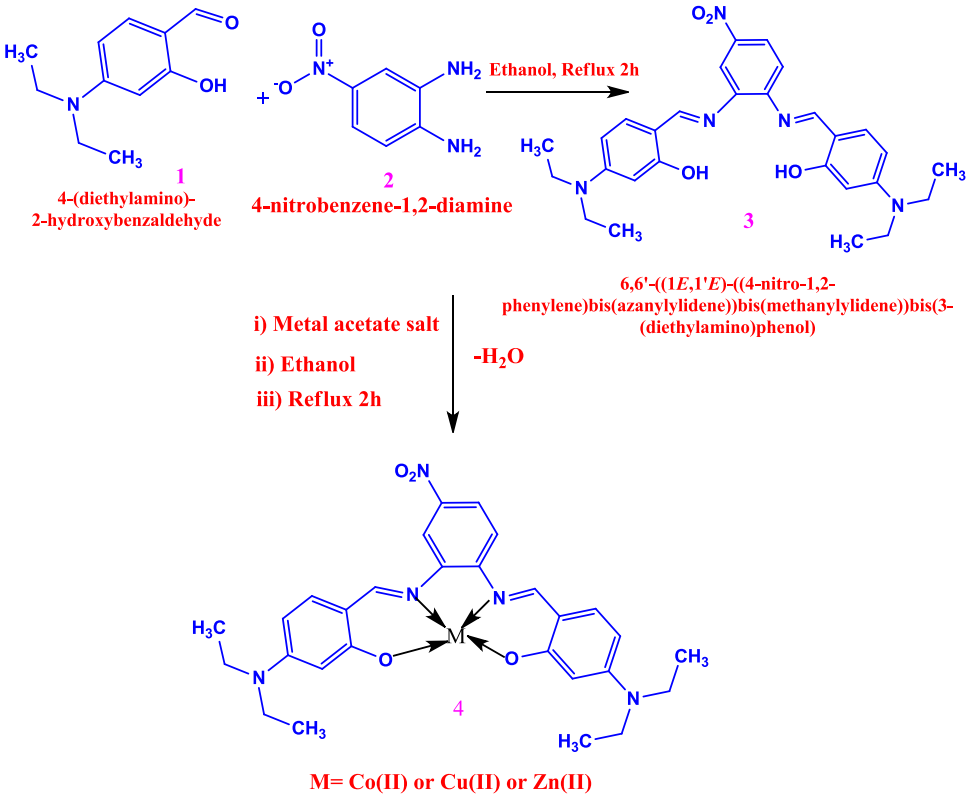

form this moiety. Antimicrobial agents have proven to be effective in the treatment of bacterial infections; however, the emergence of antibiotic resistance is a major source of concern. In light of this, it is essential that the design and synthesis of new compounds utilize cutting-edge techniques. Metal complexes have a lot of potential in terms of activity. According to the activities, Schiff base ligands and their metal complexes have very important applications in the pharmaceutical, biomedical, and electrical fields.[24−36] The developments in computational chemistry, molecular modeling, and docking have accelerated transition-metal chemistry discovery, thereby making screening for subsequent electronic structure property predictions efficient in the recent past.[30−36]

As a continuation of this research, a new Schiff base ligand was synthesized from 4-(diethylamino)-2-hydroxybenzaldehyde and 4-nitrobenzene-1,2-diamine, as well as their complexed Co (II), Cu (II), and Zn (II) ions, and their structural features were addressed. The antibacterial, antioxidant, and electrochemical features of the ligand and its associated complexes have been thoroughly investigated and addressed. Furthermore, H_2L and its complexes of CoL, CuL and ZnL were docked with the breast cancer-associated target protein HER2.

2.0. EXPERIMENTAL SECTION

The chemical compounds 4-nitrobenzene-1,2-diamine and 3-hydroxybenzaldehyde were purchased from Sigma-Aldrich and put to use without undergoing any additional purification processes. The FT-IR spectra of H_2L and its complexes CoL, CuL, and ZnL were documented using a Shimadzu FT−IR spectrophotometer IR Affinity^{-1} (1 cm^{-1} resolution) assisted by the KBr pellet method in between 4000 and 400 cm^{-1}. The ^{1}H and ^{13}C NMR isotropic shifts were visualized using a Bruker's AVANCE III 500 MHz (AV 500) at SAIF, Chennai. C, H, and N elemental analyses were conducted using an Elementar Vario EL III instrument from SRM University. H_2L and its complexes were synthesized using the described procedure.

2.1. Synthesis of the Ligand and Metal Complexes. The ligand (H_2L) was synthesized by refluxing an equimolar amount of 4-nitrobenzene-1,2-diamine and 3−4-(diethylamino)-2-hydroxybenzaldehyde in a 40 mL ethanol solution. A few drops of glacial acetic acid were added into the organic phase reaction, which was subjected to continuous agitation for a duration of 2 h. The yellowish precipitate that formed was filtered, washed with warm methanol, and vacuum-dried. The metal complexes cobalt(II), copper(II), and zinc(II) were synthesized in a 1:1 ratio (metal:Schiff base ligand). Cobalt(II) acetate, copper(II) acetate, or zinc(II) acetate salt and 25 mL of methanol were added to a round-bottom flask and vigorously stirred. A warming solution of methanol (20 mL) of Schiff base ligand (0.396 g, 2 mol) was added dropwise and agitated with heat for 4 h. Precipitates formed during cooling were filtered, cleaned using ethanol, and dried out in vacuum desiccators. Scheme 1 depicts the complex's proposed structure. The metal complexes and ligand were soluble in methanol and DMF solvent.

2.2. Computational Calculation. The Gaussian 09W[37] computational tool was used to carry out the stated computations. The optimized structural parameters of H_2L, CoL, CuL, and ZnL were obtained using DFT. Geometrical optimization and vibrational frequency calculations of the ligand and their complexes were performed utilizing the B3LYP/6-31G (d,p) functional. Time-dependent density functional theory (TD-DFT) was employed to predict the electronic UV−vis spectrum.[23−26] Vibrational analysis was

https://doi.org/10.1021/acsomega.3c08526
ACS Omega 2024, 9, 8123−8138

Table 1. Elemental Analysis and Physical Data of Studied Compounds

compound	% yield	M.P. (°C)	analysis, found (Cal.) % C	H	N	O	M	Mol. Wt.
$C_{28}H_{33}N_5O_4$ (H2L)/yellow	84	234	66.92 (66.78)	6.64 (6.61)	14.02 (13.91)	(12.14)		503.59
$C_{28}H_{31}CoN_5O_4$ (CoL)/brown	78	236	60.54 (60.01)	5.06 (5.57)	12.94 (12.49)	(11.12)	11.12 (10.51)	560.51
$C_{28}H_{31}CuN_5O_4$ (CuL)/dark green	81	243	61.44 (59.51)	5.62 (5.53)	13.06 (12.39)	(11.18)	11.41 (11.24)	565.12
$C_{28}H_{31}N_5O_4Zn$ (ZnL)/light yellow	76	241	61.04 (59.32)	5.78 (5.51)	12.91 (12.35)	(11.14)	11.98 (11.53)	566.96

carried out using total energy distribution assignments assigned by the vibrational energy distribution analysis program.[38] The geometrical structure FMO descriptors of HOMO and LUMO energies were also computed through the same calculation method. The chemical reactivity parameters were determined for the ligand and metal complexes using the same level of theory.

2.3. Molecular Docking. The inhibitory nature of the H_2L, CuL, ZnL, CoL, and ligand molecules against the breast cancer-associated target protein HER2 [PDB: 3MZW] was examined using molecular docking assessment. Molecular docking evaluation was carried out with the aid of the AUTODOCK 4.0.1 program.[39] The PyMOL molecular graphics system (version 1.7.4.5 Edu) was used to visualize the docked poses of the ligand−protein complex.[40] The RCSB PDB layout was used to determine the structure of the protein under investigation.[41] The PDB files for the ligand molecules (H_2L, CuL, ZnL, and CoL) were generated based on the optimized molecular structure of each respective molecule.

3.0. RESULTS AND DISCUSSION

The resulting ligand and its tetradentate complexes are colored in nature and have acute melting points. The synthesized compounds are readily soluble in DMSO, DMF, and $CDCl_3$. The amounts of cobalt (11.12%), copper (11.44%), and zinc (12.12%) estimated using pyrolytic, colorimetric, and volumetric methods are in good accordance with the calculated values for the complexes, which can confirm the structure. Table 1 shows the relative amounts of CHN, physical measurements, and molar conductivity of H_2L, CoL, CuL, and ZnL. Scheme 1 shows the suggested structure of cobalt, copper, and zinc metal complexes.

3.1. Electronic and Magnetic Properties. The ultraviolet−visible absorption spectral analysis serves to investigate charge transfer phenomena within the molecular structure.[42−47] In DMSO solvent, the electronic UV−vis spectra of H_2L, CoL, CuL, and ZnL are obtained in the range between 200 and 800 nm. To compare the experimental UV−vis spectra results, the TD-DFT method and B3LYP/6-31G (d,p) basis set were used, providing a precise figure for the absorption wavelengths (Figure S1). The UV−vis spectra of H_2L, CoL, CuL, and ZnL, as well as significant peaks, are shown in Figure 1, and the corresponding values are tabulated in Table 2. In general, ligand-induced transitions were observed in the ultraviolet (UV) region, whereas d−d transitions were observed in the visible region. The bands caused by −CH=N are visible due to charge transfer from the interaction of the M-L electrons. Bands have been identified at wavelengths of 303 and 365 nm attributed to the $\pi \rightarrow \pi^*$ and n $\rightarrow \pi^*$ electronic transitions of H_2L.

The UV−vis main peaks at 348 and 462 nm could be assigned to the $\pi \rightarrow \pi^*$ and n $\rightarrow \pi^*$ ($^4A_2{}^F \rightarrow {}^4T_1{}^F$) & ($^4A_2{}^F \rightarrow {}^4T_1{}^P$) d−d transition states, indicating a square planar geometry structure around the cobalt(II) ion. The magnetic

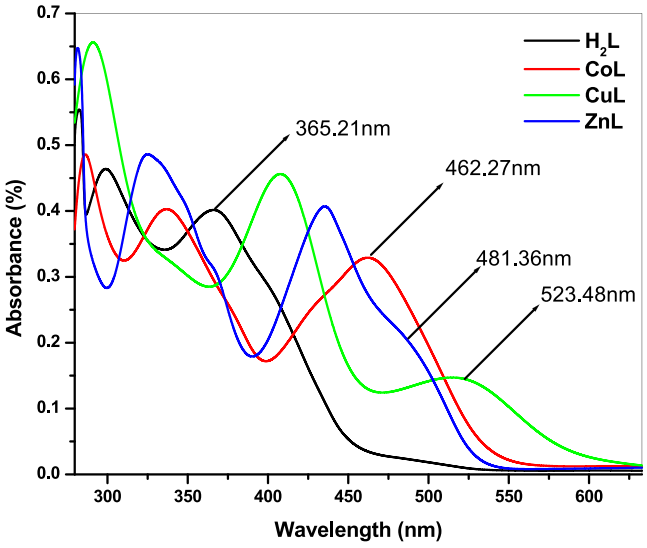

Figure 1. UV−vis spectra of H_2L and metal complexes.

Table 2. Electronic Transition Assignment and Magnetic Moment of the Studied Compounds

L/ML	absorbance (nm)	assignment	μ_{eff} BM Exp. (Cal.)
H_2L	303, 365	$\pi \rightarrow \pi^*$, n$\rightarrow\pi^*$	
CoL	286, 348, 462	$\pi \rightarrow \pi^*$, n$\rightarrow\pi^*$, LMCT	4.48 (3.86)
CuL	298, 404, 523	$\pi \rightarrow \pi^*$, n$\rightarrow\pi^*$, LMCT	1.45 (1.72)
ZnL	326, 428, 481	$\pi \rightarrow \pi^*$, n$\rightarrow\pi^*$, LMCT	diamagnetic

moment of the Co(II) complex was calculated and found as 4.48 μ_B, which is also liable for the expected square planar geometry. The presence of medium intensity bands at 404 and 523 nm in the electronic spectra of the Cu(II) complex was ascribed to the $\pi \rightarrow \pi^*$, L → M (LMCT), and d−d transitions ($^1A_1g \rightarrow {}^1A_2g$), which signifies a square planar geometry. Furthermore, the magnetic moment value was determined as 1.45 μ_B, indicating that the Cu(II) complex also had a square planar geometry. The absorption spectra peaks of ZnL observed at 428 and 481 nm are due to the $\pi \rightarrow \pi^*$ and n $\rightarrow \pi^*$ transitions. The d−d transition does not occur in the ZnL complex because all electrons are paired in the main orbital, and the complex assigns charge transfer transitions from ligand to metal and vice versa. Furthermore, the possible electronic transition and orbital contributions for both ligands and their metal complexes were calculated (Table 3), which supported the experimental results.

3.2. Vibrational Spectra. The theoretical IR spectrum of H_2L was simulated in the gaseous phase using the B3LYP/6-31G (d,p) basis level (Figure S2, tabulated in Tables 4 and 5). The FT-IR spectra of H_2L and its metal complexes are shown in Figure 2. The C−H stretching vibrational modes are frequently seen in the 3100−3000 cm^{-1} region.[48−53] For H_2L, the C−H stretching vibrations were observed at 3093 and

https://doi.org/10.1021/acsomega.3c08526
ACS Omega 2024, 9, 8123−8138

Table 3. Dipole Moments (μ), Maximum Absorption Wavelengths (λ_{max}), Oscillator Strengths (f), and Major Contribution (%) of the Studied Compounds

ligand/complexes	parameters						
	E_{total} (a.u.)	dipole moment (eV)	λ_{max} (intensity)	oscillator strength (f)	transition energy (eV)	electronic transition	major % contribution
H_2L	−273.15023	10.5631	313.21	2.251	2.251	H → L	92.86%
			476.52	0.3228	2.4575	H − 1 → L	95.26%
CoL	−2300.4163	5.293	298.45	0.1984	3.0251	H → L	94.38%
			356.18	0.0129	2.0314	H → L + 1	88.62%
			472.95	0.0164	1.1286	H − 2 → L	92.12%
CuL	−3283.7756	7.8597	303.14	0.4513	1.2772	H − 1 → L	88.12%
			398.66	0.0635	1.4978	H → L + 1	88.96%
			526.28	0.4531	2.413	H − 1 → L	92.14%
ZnL	−3439.2674	11.8786	342.12	0.0059	1.5467	H → L	92.28%
			429.36	0.1693	1.8357	H → L + 2	81.52%
			486.24	0.4184	2.1369	H − 1 → L	96.24%

3055 cm^{-1}, the in-plane bending vibration occurs in 1331, 1174, and 1126 cm^{-1}, and the out-of-plane bending vibrations originated at 958, 844, 764, and 671 cm^{-1}. The CH_3 asymmetric and symmetric stretching vibrational modes were found at 2994 and 2972 cm^{-1}; in addition, the CH_2 asymmetric and symmetric stretching vibrational modes were found at 2916 and 2895 cm^{-1}. The observed results are in good agreement with previous literature studies.[6,8] The calculated C−H stretching bands are observed at 3093 and 3058 cm^{-1}, respectively, whereas the asymmetric and symmetric stretching modes for CH_3 were found at 2996 and 2975 cm^{-1}. Similarly the symmetric and asymmetric stretching vibrational spectra for CH_2 were identified at 2914 and 2895 cm^{-1}, respectively. The CH_2 and CH_3 rocking modes were found at 1428 and 1381 cm^{-1}, respectively. The CO stretching vibrational band[50] was found at 1364 cm^{-1}, while the in-plane bending (C−OH) band originated at 1288 cm^{-1}, whereas the out-of-plane bending vibration appeared at 1064 cm^{-1}. The vibrational bands between 990 and 1585 cm^{-1} are caused by the C−N bands. The CN stretching vibrational modes were found at 1092 and 1051 cm^{-1}.[53] The bending assignments of CNC and NCC were exhibited at 612 and 518 cm^{-1}. The NO_2 stretching vibrational mode was found at 1575 cm^{-1}, whereas the bending band originated at 634 cm^{-1}. The experimental vibrational frequencies are closely correlated with the calculated modes (Table 3). The HC=N functional group exhibits a reduction in double bond character due to a pair of valence electrons donated from azomethine nitrogen to the vacant orbitals of the metal atoms. The coordination of a ligand with metals involves phenolic oxygen as an additional coordination site. In addition, the appearance of relatively faint peaks at lower wavenumbers, which can be attributed to the presence of M−N and M−O bonds, indicates the occurrence of chelation involving azomethine nitrogen and phenolic oxygen. CoL, CuL, and ZnL C=N stretching vibrational frequencies were found at 1578, 1594, and 1562 cm^{-1}.

The calculated C=N stretching bands at 1584, 1596, and 1571 cm^{-1} are closely related to the observed experimental bands. In addition, CO stretching vibrational bands were found at 1279 (CoL), 1296 (CuL), and 1258 cm^{-1} (ZnL). The M−O stretching modes are also found at 544 (CoL), 579 (CuL), and 518 cm^{-1} (ZnL). Furthermore, the M−N stretching vibrational modes of CoL, CuL, and ZnL were found at 496, 522, and 478 cm^{-1}. The experimental bands correlate well with the calculated bands. The computed CO stretching modes are 1284 cm^{-1} (CoL), 1301 cm^{-1} (CuL), and 1266 cm^{-1} (ZnL), whereas the calculated M−N stretching modes are found at 504 cm^{-1} (CoL), 528 cm^{-1} (CuL), and 476 cm^{-1} (ZnL) (refer to Figure S2). Moreover, the vibrational bands observed in this study have been correlated with previous reports.[6,8]

3.3. NMR Spectra. The quantity and composition of atoms in a compound can be identified by examining its nuclear magnetic resonance (NMR) spectrum and calculating their proportions throughout the compound's immediate environment.[54−57] The absorption peak in an NMR spectrum is determined by comparing the resonance frequency of a nucleus to a reference value. The NMR spectra of the ligand were acquired using $CDCl_3$ as the solvent, whereas those of the metal complexes were obtained using DMSO. The NMR spectra of the ligand and its transition complexes are shown in Figures S3−S8. The phenolic protons H65 and H67 appeared at 12.263 and 11.015 ppm, and the azomethine protons H29 and H70 were found at 8.691 ppm. The aromatic proton ^1H NMR multiple peaks were found at the 7.44−6.99 ppm regions. The CH_2 protons were found at 2.047 ppm, while the methyl protons were observed at 1.57 to 1.25 ppm. The azomethine carbon C7 and C69 chemical shifts were found at 164.14 ppm, and those of the phenolic carbons C13 and C17 were at 192.21 ppm. In addition, the aromatic carbons were assigned at 148.04−116.04 ppm, while few aromatic carbons were found at 98.21−89.14 ppm. This could be due to higher electronegativity groups present in the aromatic rings. Furthermore, the aliphatic carbons were also found at 36.14 and 21.98 ppm. Metal complex azomethine protons H29 and H68 were assigned at 8.89 and 8.80 ppm (CoL) and 8.43 ppm (CuL). The CoL aromatic protons were found at 7.64−6.93 ppm, while aliphatic protons were found at 2.43 and 1.04−1.00 ppm. The CoL and CuL azomethine carbons C7 and C67 were found at 164.08 and 160.62 ppm, respectively, while the CoL aromatic carbons were noticed at 149.95−115.96 ppm and aliphatic carbons at 39.79−25.02 ppm. CuL aromatic protons are found at 7.31−7.07 ppm, while aliphatic protons are found at 2.43−1.00 ppm. The methyl protons were found at 1.19−0.99 ppm, while the CH_2 protons were found at 3.42−3.37 ppm. The CuL aromatic carbons were found at 149.96−115.97 ppm, while aliphatic carbons originated at 40.62−14.49 ppm.

3.4. Mass Spectra. Mass spectrometry is widely acknowledged as a potent technique for the structural elucidation of molecules within the domain of molecular chemistry. The

https://doi.org/10.1021/acsomega.3c08526
ACS Omega 2024, 9, 8123−8138

Table 4. Assignments of Fundamental Vibrations of H_2L[a]

S.No.	Exp.	calculated	scaled	IR intensity	PED
1	3654	3700	3648	3.10	υOH(100)
2	3458	3501	3452	37.49	υOH(100)
3	3093	3143	3099	0.11	υCH(87)
4		3142	3098	0.98	υCH(62)
5		3135	3091	2.10	υCH(95)
6		3134	3090	2.08	υCH(86)
7		3126	3082	0.20	υCH(73)
8		3114	3070	0.78	υCH(94)
9		3105	3062	0.05	υCH(99)
10	3055	3101	3058	1.95	υCH(98)
11		3069	3026	0.91	υCH(97)
12		3040	2997	9.14	υCH(53)
13	2994	3039	2996	8.86	υCH_3(75)
14		3034	2992	0.84	υCH(63)
15		3033	2991	0.58	υCH(65)
16		3026	2984	1.69	υCH(78)
17		3022	2980	5.02	υCH(58)
18		3021	2979	4.92	υCH(51)
19		3019	2977	5.91	υCH(62)
20	2972	3017	2975	6.44	υCH_3(99)
21		3002	2960	1.85	υCH(65)
22		3001	2959	2.18	υCH(69)
23		2994	2952	0.16	υCH(71)
24		2991	2949	0.36	υCH(62)
25		2970	2928	2.13	υCH(55)
26	2916	2955	2914	9.47	υCH_2(95)
27		2953	2912	6.96	υCH(71)
28		2949	2908	2.39	υCH(51)
29		2944	2903	3.18	υCH(77)
30		2937	2896	4.52	υCH(66)
31	2895	2935	2894	4.47	υCH_2(86)
32		2934	2893	1.51	υCH(75)
33		2933	2892	1.10	υCH(99)
34	1612	1631	1608	81.04	υN=C(23)
35		1615	1592	17.25	υCC(15)
36	1575	1596	1574	36.47	υNO_2(24)
37		1573	1551	37.72	υN=C(16)
38		1557	1535	58.62	υCC(26)
39		1547	1525	29.34	υNC(26)
40		1540	1518	30.67	σHCN(11)
41		1533	1512	59.29	υCC(17)
42		1510	1489	20.71	υCC(13)
43		1502	1481	29.61	υCC(13)
44		1497	1476	1.84	υCC(29)
45	1472	1494	1473	21.25	υCC(11)
46	1468	1484	1463	9.82	υNC(24)
47		1483	1462	0.79	γHCC(10)
48	1452	1477	1456	0.71	υCC(22)
49		1475	1454	0.30	γHCH(18)
50		1468	1447	0.02	γHCH(32)
51		1467	1446	0.55	γHCH(27)
52		1461	1441	1.79	γHCC(14)
53		1461	1441	0.60	γHCH(27)
54		1457	1437	6.30	γHCH(26)
55		1455	1435	0.52	γHCH(25)
56		1454	1434	0.33	γHCH(31)
57	1428	1446	1426	13.16	$\mathrm{rocCH_2}$(34)
58		1427	1407	1.52	γHCH(17)
59		1412	1392	3.41	γHCH(23)
60	1381	1402	1382	10.92	$\mathrm{rocCH_3}$(25)
61		1387	1368	16.09	γHCH(19)
62		1386	1367	2.13	γHCH(18)
63		1383	1364	2.28	γHCH(12)
64		1381	1362	0.53	γHCC(17)
65	1364	1380	1361	3.19	υCO(25)
66		1373	1354	4.65	γHCH(24)
67		1372	1353	15.15	τHCCN(10)
68		1364	1345	0.27	υCC(24)
69	1331	1351	1332	4.02	γHCC(12)
70		1349	1330	0.35	υCC(11)
71		1343	1324	21.00	υCC(10)
72		1340	1321	19.17	σHCN(10)
73		1336	1317	10.27	υNC(12)
74		1336	1317	1.10	γHCC(13)
75		1335	1316	13.95	τHCNC(11)
76		1317	1299	0.87	υCOH(18)
77	1288	1298	1280	13.07	γCOH(19)
78		1290	1272	2.32	σHCN(15)
79		1282	1264	1.31	τHCNC(16)
80		1277	1259	2.15	τHCNC(16)
81		1272	1254	12.94	τHCNC(17)
82		1256	1238	5.07	τHCNC(24)
83		1251	1233	6.22	τHCNC(13)
84		1247	1230	16.24	τHCNC(21)
85		1240	1223	23.75	σHCN(30)
86		1212	1195	1.27	σCCC(14)
87		1209	1192	100.00	σCCC(22)
88		1204	1187	33.89	σCCC(11)
89	1174	1190	1173	3.17	γHCC(23)
90		1188	1171	4.04	τHCNC(10)
91		1183	1166	7.31	σHCN(26)
92		1164	1148	9.43	σCCC(20)
93		1150	1134	0.20	τCCCC(11)
94		1146	1130	4.17	vHCC(14)
95	1126	1136	1120	23.99	γHCC(16)
96		1124	1108	17.03	υOC(26)
97	1092	1110	1094	4.85	υNC(12)
98		1085	1070	2.51	υOC(15)
99	1064	1084	1069	3.35	βCOH(18)
100		1077	1062	9.90	υNC(15)
101		1075	1060	4.80	υNC(12)
102		1072	1057	3.56	υNC(14)
103	1051	1067	1052	14.88	υNC(15)
104		1054	1039	0.08	υNC(17)
105		1053	1038	0.07	υNC(19)
106		1002	988	1.02	γHCC(14)
107		1001	987	3.83	τHCCN(13)
108		999	985	8.68	τHCCN(12)
109		987	973	0.23	τHCCN(11)
110		984	970	1.16	τHCCN(18)
111	958	977	963	3.04	βHCCC(24)
112		946	933	4.92	τHCCN(10)
113		943	930	6.36	βHCCC(21)
114		941	928	0.54	τHCCN(13)
115		938	925	0.30	τCCCC(15)
116		922	909	2.75	τCCCC(15)
117		919	906	3.16	τCCCC(19)
118		900	887	0.15	τCCCC(16)
119		900	887	0.25	βHCCC(11)
120		866	854	1.11	τHCNC(25)
121		854	842	3.87	βHCCC(33)
122	844	853	841	4.37	βHCCC(29)

https://doi.org/10.1021/acsomega.3c08526
ACS Omega 2024, 9, 8123−8138

Table 4. continued

S.No.	Exp.	calculated	scaled	IR intensity	PED
123		844	832	1.83	τCCCC(19)
124		827	815	6.86	τCCCC(10)
125		823	811	3.88	τHCNC(52)
126	802	809	798	0.24	βHCCC(12)
127		806	795	0.31	τHOCC(26)
128		796	785	2.67	τHCCN(17)
129		777	766	0.57	τCCCC(22)
130		776	765	1.09	σCCC(16)
131		775	764	1.63	τCCCC(10)
132	764	772	761	14.69	βHCCC(28)
133		767	756	0.85	τCCCC(12)
134		752	741	1.80	τCCCC(11)
135		749	739	1.21	τHCCN(56)
136		735	725	0.19	τCCCC(15)
137		719	709	0.12	σNCC(10)
138		699	689	1.75	τHCCN(15)
139	671	683	673	1.11	βHCCC(11)
140		670	661	3.03	τCCCC(10)
141		649	640	0.45	τHCCN(13)
142	634	645	636	0.27	σONO(20)
143		634	625	0.62	τHCCN(18)
144	612	615	606	0.05	σCNC(20)
145		594	586	1.18	τCCCC(10)
146		565	557	0.05	τOCCC(11)
147		547	539	0.58	τNCCC(13)
148		544	536	0.64	τNCCC(18)
149		539	531	0.28	τCCCC(10)
150	518	533	526	0.40	σNCC(13)
151		523	516	2.90	τOCON(60)
152		507	500	0.49	τNCCC(15)
153		492	485	1.10	σCCC(14)
154		477	470	0.75	σCCC(10)
155		474	467	0.34	τCCCC(11)
156		471	464	0.02	σCCC(13)
157		461	455	0.01	σCCC(22)
158		444	438	0.42	σCCC(10)
159		435	429	1.79	σCCC(10)
160		430	424	0.28	τOCCC(27)
161		425	419	0.76	σCCC(11)
162		402	396	0.43	σNCC(14)
163		381	376	0.80	σCNC(12)
164		378	373	0.39	σCCC(13)
165		363	358	0.15	σCNC(11)
166		360	355	0.59	σCCC(10)
167		343	338	0.23	σONC(12)
168		310	306	9.95	σCNC(12)
169		296	292	2.29	τNCCC(11)
170		293	289	0.04	σCNC(13)
171		286	282	1.21	σCCN(17)
172		282	278	0.88	σCCN(10)
173		259	255	0.09	σCCN(10)
174		256	252	0.13	σOCC(37)
175		230	227	0.50	σOCC(11)
176		229	226	0.04	σCCN(11)
177		225	222	0.18	τCCCN(13)
178		218	215	0.10	σNCC(11)
179		214	211	0.11	τHOCC(61)
180		208	205	0.09	σCCN(16)
181		206	203	0.19	σNCC(12)
182		195	192	0.04	τCCCC(12)
183		186	183	0.05	τCCCC(19)
184		173	171	0.34	σNCC(14)
185		160	158	0.34	τNCCC(11)
186		145	143	0.04	τCCCC(13)
187		128	126	0.04	τCCNC(10)
188		124	122	0.16	σCNC(10)
189		108	106	0.03	τCCNC(12)
190		99	98	0.00	τCCCN(26)
191		95	94	0.04	τCNCC(14)
192		93	92	0.11	τCCCN(32)
193		85	84	0.12	τCCNC(51)
194		71	70	0.08	τCCNC(31)
195		65	64	0.09	τCNCC(18)
196		54	53	0.01	τCCNC(28)
197		45	44	0.08	τONCC(24)
198		41	40	0.04	σCNC(12)
199		38	37	0.02	τCNCC(14)
200		31	31	0.02	τCCCC(11)
201		24	24	0.00	τCCNC(15)
202		19	19	0.01	τCNCC(15)
203		17	17	0.04	τCCCN(11)
204		11	11	0.02	σCCN(12)

[a]Symbol: υ → stretching, γ → in-plane bending, β → out-of-plane bending, σ → bending, τ → torsional.

Table 5. Important Experimental and Calculated Stretching Vibrational Frequencies (cm^{-1}) of H_2L and Metal Complexes

metal complex	vibrational assessments			
	C=N	C−O	M−O	M−N
CoL	1578 (1591)	1279 (1284)	544 (542)	496 (492)
CuL	1594 (1612)	1296 (1298)	579 (581)	522 (528)
ZnL	1562 (1568)	1258 (1271)	518 (512)	478 (473)

utilization of this approach has proven to be highly effective in the field of coordination chemistry, specifically in determining the primary molecular ion peaks within the Schiff base complexes that have been synthesized. The analysis was performed by utilizing the mass spectrometry technique known as electrospray ionization mass spectrometry (ESI-MS). The molecular ion peaks observed in the mass spectra of H_2L, CoL, CuL, and ZnL exhibit strong agreement with the values calculated, as depicted in Figures S9−S12. An observed peak with a mass-to-charge ratio (m/z) of 503.1421 was identified, which could potentially be attributed to the deprotonated form of the ligand. The mass spectra of the metal complexes CoL, CuL, and ZnL exhibited a fragmentation ion peak with m/z values of 560.1897, 563.4556, and 565.1206, respectively. These peaks are potentially indicative of the parent molecular ion peak.

3.5. X-ray Powder Diffraction. The powder X-ray diffraction (XRD) of samples exhibited distinct and well-defined crystalline peaks, which serve as evidence of their crystalline phase.[54−56] The distinction between the Schiff base

https://doi.org/10.1021/acsomega.3c08526
ACS Omega 2024, 9, 8123−8138

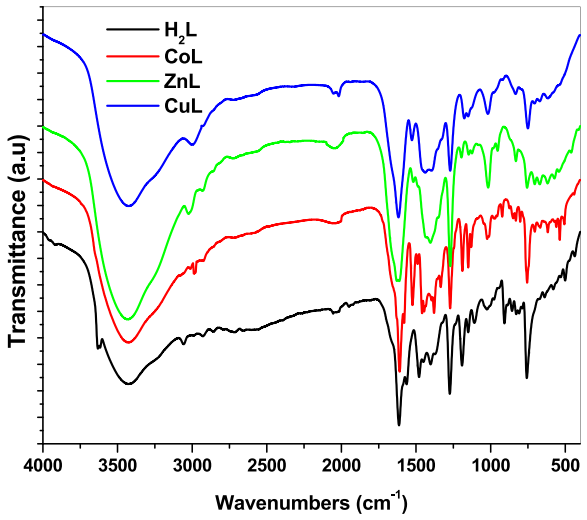

Figure 2. FT-IR spectra of H_2L and metal complexes.

design and the metal complexes becomes apparent due to the formation of distinct crystalline phases.

The powder XRD patterns of H_2L, CoL, CuL, and ZnL complexes recorded in the range 2θ = 10−90° are shown in Figure 3. The average crystallite sizes of the CoL, CuL, and ZnL complexes are 61, 74, and 49 nm, respectively.

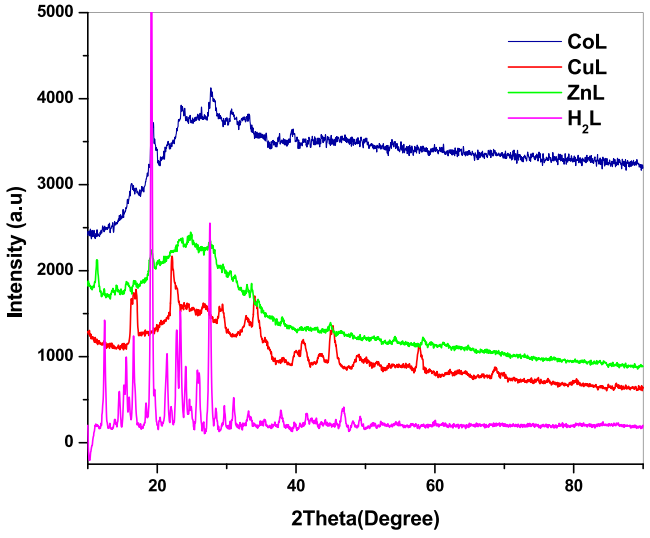

Figure 3. Powder X-ray diffraction of the ligand and metal complexes.

3.6. Cyclic Voltammetric Study. The cyclic voltammetric method was employed to investigate the redox behavior of cobalt, copper, and zinc (Figure 4) in both coordinated and uncoordinated states.[S4] The CoL metal complex exhibited a cathodic peak at a potential of 1.216 V and an anodic peak at −0.428 V. The cyclic voltammograms obtained for both electroactive species demonstrate the occurrence of a two-electron transfer mechanism

$$Co^{2+} \rightarrow Co^{0} \quad (1)$$

$$Co^{0} \xrightarrow{+2e} Co^{2+} \quad (2)$$

The CuL metal complex exhibited a cathodic peak at a potential of 0.285 V and an anodic peak at 0.498 V. The cyclic voltammograms obtained for both electroactive species

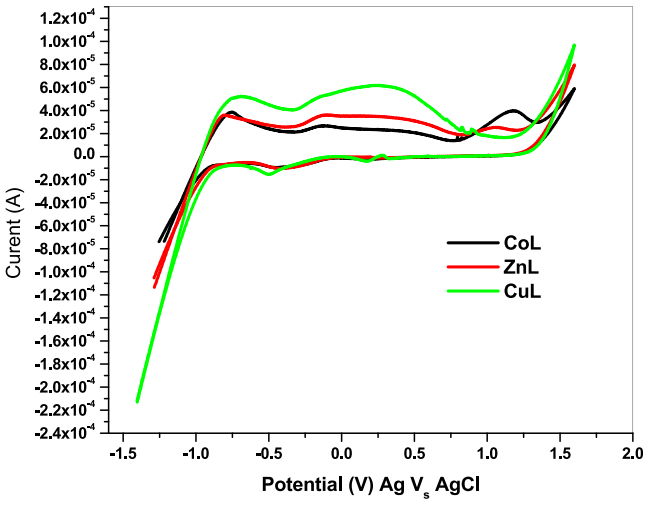

Figure 4. Cyclic voltammograms of Co(II), Cu(II), and Zn(II) complexes.

demonstrate the occurrence of a two-electron transfer mechanism

$$Cu^{2+} \rightarrow Cu^{0} \quad (3)$$

$$Cu^{0} \xrightarrow{+2e} Cu^{2+} \quad (4)$$

The ZnL complex exhibits a cathodic peak at a potential of 1.125 V and an anodic peak at a potential of 0.486 V. The electron transfer mechanism can be described as a single-step process

$$Zn^{2+} \rightarrow Zn^{0} \quad (5)$$

$$Zn^{0} \xrightarrow{+2e} Zn^{2+} \quad (6)$$

The magnitudes of the cathodic and anodic peak currents observed in the voltammogram of the metal complex are notably diminished compared with those observed in the voltammogram of the metal salt.

3.7. Electron Paramagnetic Resonance (EPR). The EPR spectra of the Cu (II) complex offer crucial information for investigating the natural environment of metal ions. Figure 5 illustrates the EPR spectra of the Cu(II) complex obtained in DMSO at ambient temperature (300 K) and at liquid nitrogen (77K). The S1 signal, which possesses a well-resolved hyperfine structure and axial symmetry (g‖(S1) = 2.19451; g⊥(S1) = 2.06759), showed the existence of an unpaired electron in the $d_{x^2-y^2}$ orbital. The results indicated the presence of covalent nature of the metal−ligand bond with isolated Cu(II) ions occupying square planar positions.

3.8. Molecular Structure. Geometry optimization is significant due to the crucial role it serves, which is to execute a series of iterations until a minimum value is achieved.[S7] The geometrical parameters that have been optimized for H_2L, CoL, CuL, and ZnL are determined through the utilization of B3LYP with a 6-31G (d,p) basis set. The resultant structures, accompanied by their atom numberings, are shown in Figure 6. The ground state geometrical parameters are presented in Tables S1−S4. Bond lengths and angles serve as a reliable approximation for the molecule structure design and as a basis for vibrational frequency calculations. On the other hand, dihedral angles ascertain the rotational motion of aryl rings in relation to the remainder of the molecule. The C2−C3, C1−

https://doi.org/10.1021/acsomega.3c08526
ACS Omega 2024, 9, 8123−8138

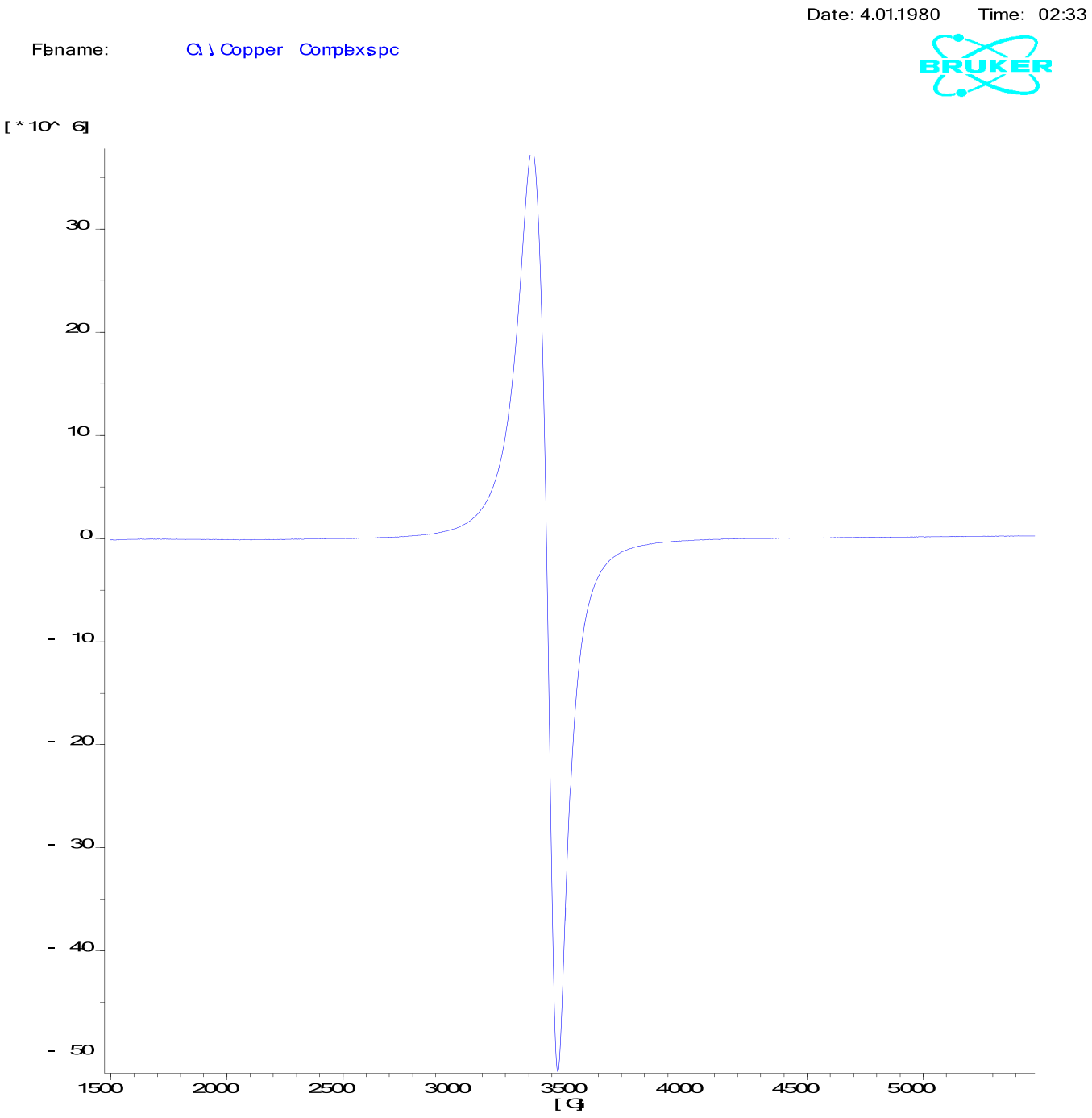

Figure 5. EPR spectra for the Cu(II) complex.

C2, C5−C6, C3−C4, C8−C9, C11−C12, C9−C10, C17−C18, C16−C17, C19−C20, and C20−C21 bond lengths (H_2L) have been calculated in the range of 1.39−1.43 Å, while the C4−C5, C10−C11, and C18−C19 bond lengths (H_2L) fall on 1.43−1.43 Å due to the inductive effect that occurs in the whole system. Further, N15−C44, N15−C61, N23−C50, and N23−C47 bond lengths are 1.48 Å, and also the highest bond length found for C36−C47, C50−C53, C40−C44, and C57−C61 (H_2L) being 1.55 Å shows a single bond character. In addition, C4−N14 and C5−N22 bond lengths of 1.42 Å indicate a single bond character, and those of C7−N14 and C69−N22 (H_2L) are 1.32 and 1.32 Å, indicating a double bond character. Moreover, the bond lengths of N24−O25 and N24−O35 (H_2L) are 1.31 and 1.32 Å, respectively. The bond lengths of N14−Co69, N22−Co69, O64−Co69, and O65−Co69 (CoL) are 1.83, 1.82, 1.81, and 1.80 Å, respectively. In addition, the bond lengths of N14−Cu69, N22−Cu69, O42−Co69, and O43−Co69 (CuL) are 1.87, 1.88, 1.88, and 1.89 Å, respectively. In addition, the bond lengths of N14−Zn47, N22−Zn47, O42−Zn47, and O43−Zn47 (ZnL) are 1.99, 1.98, 1.96, and 1.94 Å, respectively. The important bond lengths of (H_2L) C4−C5−C6, C3−C2−C1, C5−N22−C7, C4−N12−C7, C12−C11−C10, and C20−C19−C18 are 118.1, 120.6, 134.2, 122.7, 117.8, and 117.1°, respectively. In addition, the bond lengths of C17−O64−H65 and C13−O66−H67 are 112.2 and 108.4°, respectively, showing that intramolecular

https://doi.org/10.1021/acsomega.3c08526
ACS Omega 2024, 9, 8123−8138

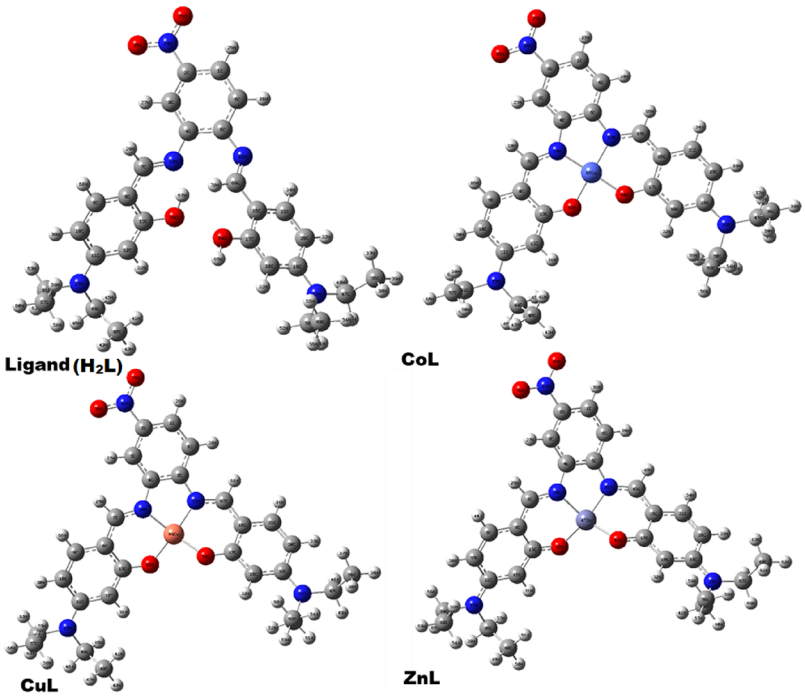

Figure 6. Optimized ligand and its metal complexes.

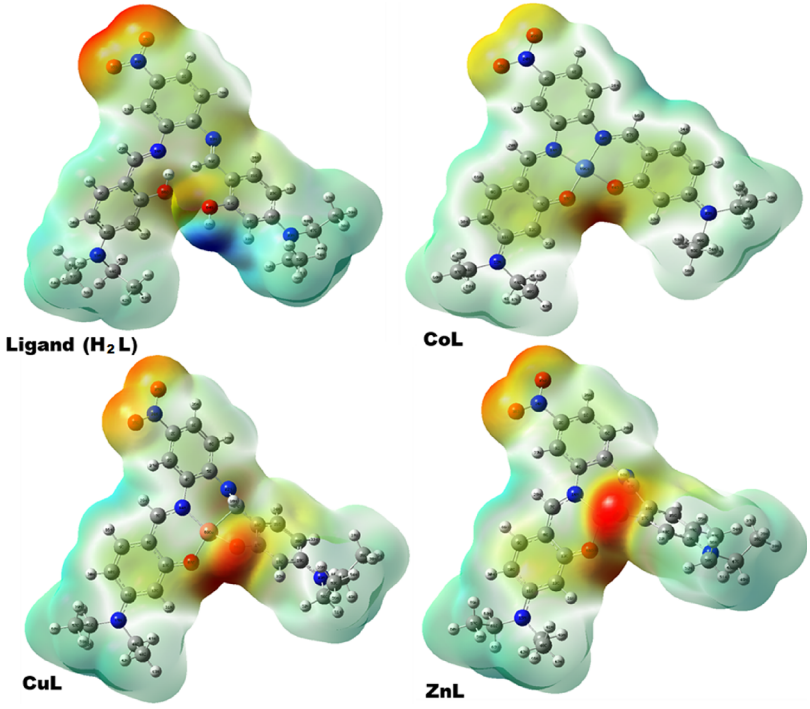

Figure 7. Molecular electrostatic potential surface of H_2L and its metal complexes.

interaction occurs in between oxygen and nitrogen atoms. The important dihedral angles obtained for C6−C1−C2-C3, C2−C1−C6−C5, C9−C8−C13−C12, C8−C9−C10−C11, C11−C12−C13−C8, C21−C16−C17−C18, C17−C16−C21−C20, C16−C17−C18−C19 being 0.3, −1.5, 0.5, −0.6, 0.3, 0.1, 0.3, and −0.7°, respectively. The bond angles of N14−Co69−N22 and O65−Co69−O64 were found to be 87.1 and 85.2°, respectively. In addition, the bond angles of N14−Cu69−N22 and O42−Cu69−O43 are 88.2 and 83.7°, respectively. The bond angles of N14−Zn47−N22 and O42−Zn47−O43 were obtained as 84.8 and 92.1°, respectively. The C4−N14−Co69−O65, C5−N22−Co−O64, C4−N14−Cu69−O43, C5−N22−Cu−O65, C4−N14−Zn47−O43, and C5−N22−Zn47−O42 dihedral angles are 177.4, 177.8, 179.6, 176.7, 166.5, and 169.6°, respectively, showing that the metal complexes occur in the square planar geometrical structure. The calculated physicochemical parameters are well correlated with the literature.

3.9. Molecular Electrostatic Potential. The molecular electrostatic potential (MEP) surface represents the spatial

https://doi.org/10.1021/acsomega.3c08526
ACS Omega 2024, 9, 8123−8138

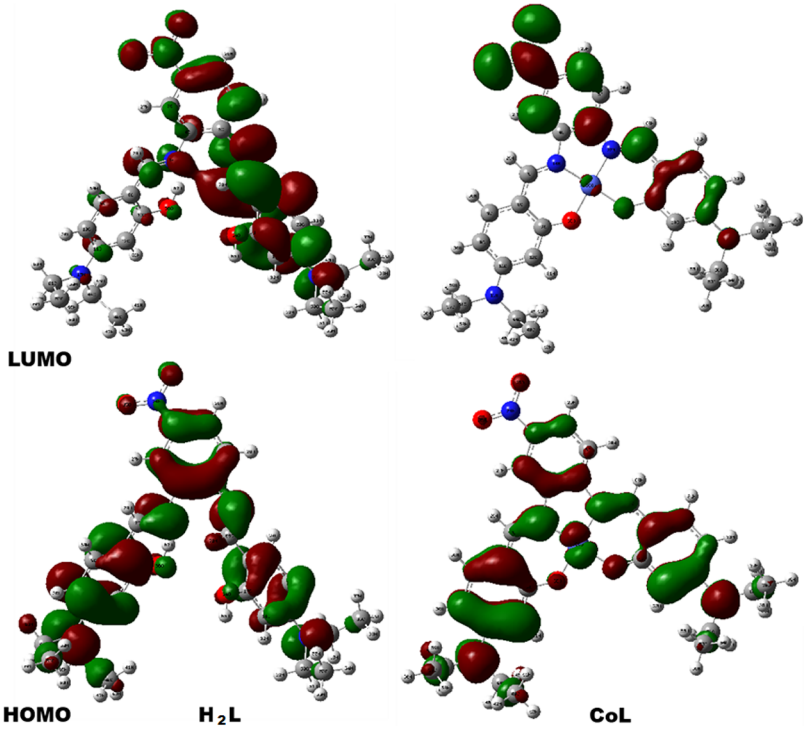

Figure 8. Frontier molecular orbitals of the ligand (H_2L) and Co(II) metal complex (CoL).

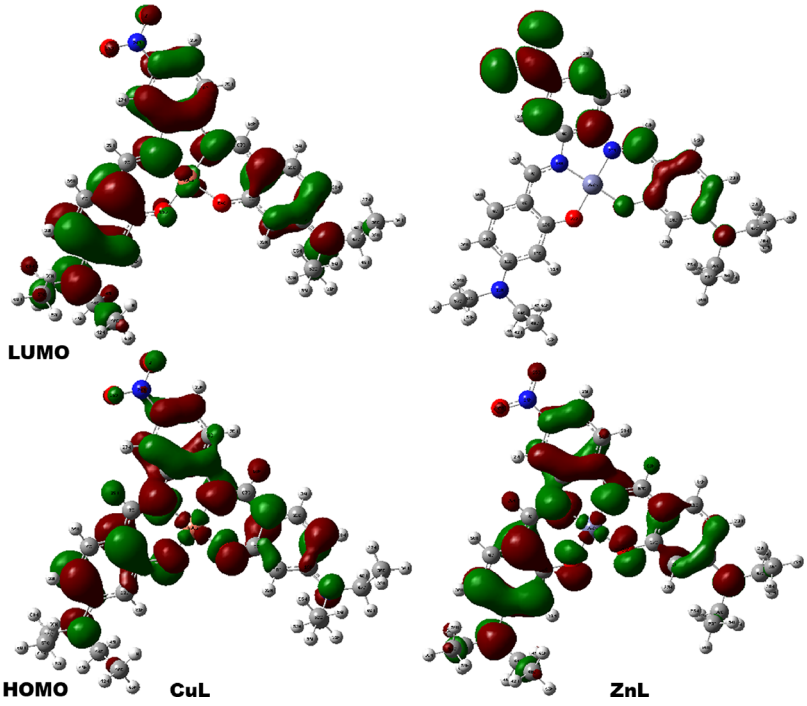

Figure 9. Frontier molecular orbitals of Cu(II) and Zn(II) metal complexes.

arrangement of electronic charge and the corresponding locations of chemical reactivity within the molecule.[50] The MEP surfaces are color-labeled in which the neutral zone is shown by green, while the positive and negative regions are represented by blue and red, respectively. On the MEP surface, the green portions indicate neutral attractions, the blue regions indicate positive electrostatic potential, and the red zone represents the greatest electronegative potentials. In Figure 7, it is clearly shown that the oxygen atom has a higher red region, showing a negative electrostatic potential and the possibility of electrophilic attack, whereas the OH proton has a higher blue region, showing a positive electrostatic potential and the possibility of nucleophilic attack for surrounding species. Within the ligand, the regions exhibiting the highest negative charge density are predominantly localized in the region of electronegative atoms (O and N). Conversely, the regions displaying the highest positive charge density are primarily situated in the vicinity of protons. In addition, the

https://doi.org/10.1021/acsomega.3c08526
ACS Omega 2024, 9, 8123−8138

Table 6. Physicochemical Parameters of the Ligand and Metal Complexes[a]

methods	L/ML	E_{HOMO}	E_{LUMO}	IP	EA	Eg	χ	μ	η	σ	ω	ε	ω+
gaseous phase	H_2L	−4.90	−2.45	4.90	2.45	2.45	−3.67	−3.67	1.22	0.82	5.51	0.18	1.78
	CoL	−5.31	−2.94	5.31	2.94	2.37	−4.12	−4.12	1.19	0.84	7.17	0.14	2.53
	CuL	−4.83	−2.43	4.83	2.43	2.40	−3.63	−3.63	1.20	0.83	5.49	0.18	1.79
	ZnL	−5.21	−2.64	5.21	2.64	2.57	−3.93	−3.93	1.28	0.78	6.00	0.17	1.94
aqueous phase	H_2L	−5.20	−2.98	5.20	2.98	2.22	−4.09	−4.09	1.11	0.90	7.53	0.13	2.78
	CoL	−5.18	−2.93	5.18	2.93	2.25	−4.05	−4.05	1.12	0.89	7.32	0.14	2.67
	CuL	−5.34	−2.91	5.34	2.91	2.43	−4.13	−4.13	1.21	0.82	7.02	0.14	2.45
	ZnL	−5.45	−3.27	5.45	3.27	2.18	−4.36	−4.36	1.09	0.92	8.71	0.11	3.34

[a]Ionization potential → IP, electron affinity → EA, η → chemical hardness, softness → σ, chemical potential → μ, electrophilicity index → ω, and nucleophilicity index → ε.

CoL, CuL, and ZnL MEP images also indicate potential reactivity. The higher red region of the oxygen atom and the smaller blue region of the methyl proton indicate electrophilic and nucleophilic attack, respectively.

3.10. Natural Bond Orbital Analysis. The NBO analysis results[58] are presented in Tables S5−S8, which include information on the natural atomic charges, populations, and electron configurations of the cobalt (Co), copper (Cu), zinc (Zn), oxygen (O), nitrogen (N), and carbon (C) atoms. The complexation process resulted in a significant decrease in the natural charge of Co, Cu, and Zn (0.9006, 1.0416, and 1.2223 kcal/mol, respectively), suggesting the occurrence of electron transfer from the orbitals of O and N to the Co, Cu, and Zn ions. The electron configuration of the cobalt, copper, and zinc ions in the complex are $4S^{0.45}3d^{7.27}4p^{0.37}5S^{0.01}$, $4S^{0.33}3d^{9.14}4p^{0.47}5S^{0.01}5p^{0.01}$, and $4S^{0.36}3d^{9.87}4p^{0.53}5p^{0.01}$, respectively. The complexed forms of Co, Cu, and Zn ions exhibit a greater occupancy of their d orbitals compared with their free ion counterparts.

The conversion of a free ion into a complex results in a marginal augmentation in the occupancy of the s-orbital. The occurrence of electron transfer to the central metal is supported by the observed increase in electron density within the s and d orbital regions of the metal ion in the CoL, CuL, and ZnL complexes. The complexes were subjected to NBO analysis (Tables S9−S12), which revealed the presence of significant electron D and A orbitals. In the present study, important interactions of C2−C3 → C4−C5 and O37 → N35−O36 stabilization energies were calculated as 99.23 and 182.07 kcal/mol, respectively, for H_2L. In the case of the CoL complex, LP (N22) → LP (Co69), C16−C67 → C17−C18, and LP (O65) → LP (Co69) had 85.4, 31.46, and 28.77 kcal/mol, respectively. For the CuL complex, those of LP(O35) → N24−O25, LP(O64) → C17−C18, C16−C67 → C17−C18, LP(N14) → Cu69, and LP(N14) → Cu69 were 81.93, 29.97, 72.77, 32.08, and 31.05 kcal/mol, respectively. Furthermore, for the ZnL complex, those of LP (C37) → N24−O25, LP (O64)) → Zn69, and LP (N24) → Zn69 were 182.66, 48.09, and 27.96 kcal/mol, respectively.

3.11. Frontier Molecular Orbital and Global Reactivity Descriptors. The primary and prevalent mechanism for energy transfer within a system involves the excitation of an electron possessing the minimum attainable energy level, as denoted by the frontier molecular orbital (FMO). The chemical stability and reactivity of organic compounds are significantly influenced by these parameters.[59−63] Charge transfer between molecules is facilitated by a compound whose molecular backbone is composed of a π-conjugated system featuring an electron-donating group and an electron-withdrawing group (refer to Figures 8 and 9). Stability information and precise estimations of the chemical reactivity of compounds are furnished by the band gap energy. The band gap energies of H_2L, CoL, CuL, and ZnL are listed in Table 6. The stability of the molecule is a critical factor in the process of designing biomedically significant drugs. A reduced energy gap results in decreased stability and increased reactivity of the molecule. A system characterized by a significant energy gap exhibits enhanced stability and reduced reactivity. The calculated energy gaps of the ligand, CoL, CuL, and ZnL in the present study are 2.45, 2.37, 2.40, and 2.57 eV (gaseous phases) and 2.22, 2.25, 2.43, and 2.18 eV (aqueous phases), respectively. When compared to previous studies, the results show that the synthesized ligand and its metal complexes exhibit greater selectivity. Furthermore, the HOMO can be conceptually understood as an orbital that donates electrons and is closely associated with the ionization potential of the system. Conversely, LUMO can be characterized as an orbital that accepts electrons and is linked to the electron affinity of the molecules (Table 6). Figures 8 and 9 reveal the donor and accept region of the ligand and CoL, CuL, and ZnL.

The ionization potential value signifies the minimum energy required to dissociate an electron from the highest occupied molecular orbital (HOMO). A lower electron affinity value suggested that the ligands, CoL, CuL, and ZnL have a greater propensity to accept electrons to form bonds. The electron affinity indicates an increased molecular reactivity with electron-donating orbitals. The recorded hardness and softness values provide confirmation of the molecule's elevated molecular softness. The identified lower chemical potential and higher electrophilicity index values are similar to those observed in bioactive molecules. The chemical potentials of H_2L, CoL, CuL, and ZnL are −4.09, −4.05, −4.13, and −4.36 eV, respectively. The observed results indicated that both the ligand and complexes demonstrate stability and resist disintegration into their fundamental constituents. According to Parr et al,[63] the parameter ω is determined by the quantities μ and η, both of which are positive. These quantities represent the energy stabilization that occurs when the system acquires an additional charge (N) from neighboring molecules. The varying magnitudes of μ and ω serve as indicators of the favorable electrophilic and nucleophilic properties exhibited by ligands and their corresponding metal complexes, respectively. Furthermore, the electrophilicity index results obtained for the complexes indicated that the CoL complex exhibits a higher electrophilic character compared to the Cu and Zn complexes. Also, it should be noted that CoL exhibited a significantly higher electronegativity value of 3.6341 eV, thereby indicating its enhanced catalytic activity.

https://doi.org/10.1021/acsomega.3c08526
ACS Omega 2024, 9, 8123−8138

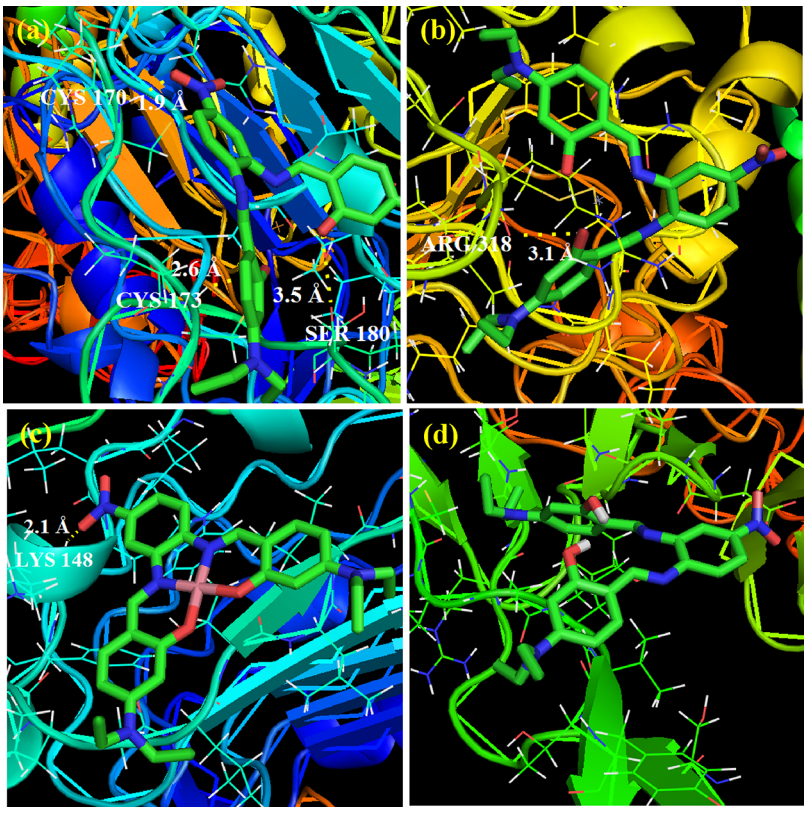

Figure 10. Lowest energy docked pose of the (a) CuL, (b) ZnL, (c) CoL, and (d) ligand docked with HER2 gene [PDB: 3MZW].

Table 7. Obtained Docking Parameters of the Molecules Docked with Target Protein HER2 [PDB: 3MZW] on Their Rank

	docking parameters based on the rank								
	binding energy (kcal/mol)			inhibition constant			intermolecular energy(kcal/mol)		
compound	1	2	3	1	2	3	1	2	3
CuL	−5.59	−5.21	−4.73	80.21 μM	151.29 μM	341.14 μM	−7.68	−7.30	−6.82
ZnL	−5.50	−5.07	−5.04	93.45 μM	192.32 μM	200.55 μM	−7.59	−7.16	−7.13
CoL	−5.34	−5.00	−4.99	122.38 μM	215.96 μM	219.02 μM	−7.43	−7.09	−7.08
H_2L	−3.67	−2.73	−2.19	2.04 mM	10.05 mM	24.69 mM	−7.55	−6.60	−6.07

3.12. Molecular Docking Analysis. Molecular docking analysis is often employed to predict the atomic interaction between the ligand molecule and a known target protein, which provides small molecule interaction behavior at target protein binding sites as well as elucidates key biochemical processes.[64,65] In recent years, H_2L-based complexes have been found to have significant anticancer activity against various cancers.[53] In this case, H_2L, CuL, ZnL, and CoL molecules were docked with breast cancer-associated target protein HER2 [PDB: 3MZW]. Figure 10 depicts the lowest energy docking pose of the H_2L molecule with the breast cancer-associated target protein.

The amino acid in the target protein molecule that participates in H-bond formation, as well as the length of the H-bonds, is depicted in Figure 10. The computed molecular docking parameters were also documented in Table 7. These results indicate that the CuL molecule has lower binding energy (−5.59 kcal/mol) and inhibition constant (80.21 μM) values against the targeted protein than other ligand molecules. Furthermore, the CuL molecule required only an 80.21 μM sample for inhibition, but the H_2L ligand required a 2.04 mM sample, indicating that Cu doping increases the bioactivity of the H_2L ligand. These results clearly show that the CuL molecule may be employed as a new inhibitor of HER2 gene activities. As a result, these findings will be valuable in the development of effective drugs for the treatment of breast cancer.

3.13. Antioxidant Activities. The antioxidant activity of the ligand and metal complexes has been investigated in relation to ascorbic acid, and comparisons were made at different concentrations ranging from 50 to 500 mM.[66−68] The results of the antioxidant activities were observed and are shown in Figure S13. Table S13 presents the antioxidant capacity of the synthesized compounds as well as the standard antioxidant (ascorbic acid) in terms of their inhibition concentration. The percentage of inhibition exhibited by the complexes is compared to that of the control and presented in the following sequence. The order of reactivity for the complexes Cu(II), Co(II), Zn(II), and H_2L is Cu(II) > Co(II) > Zn(II) > H_2L and suggests that CuL exhibits a higher level of activity compared to the other complexes. This observation aligns with the inverse relationship observed between the IC_{50} result and antioxidant capacity. The diamine derivative's nitro group substituted in the aromatic ring

https://doi.org/10.1021/acsomega.3c08526
ACS Omega 2024, 9, 8123−8138

increases the stability of the synthesized metal complexes' assembled free radicals, which increases the molecule's activity to steady unpaired electrons and scavenge radicals. The results of this study thus establish a connection between the application of the synthetic compounds in the prevention and treatment of pathological conditions brought on by oxidative stress.

3.14. Biological Properties. The biological activity of the synthesized complexes and ligand was assessed against antifungal and antibacterial agents (Figures S14 and S15), and the results are presented in Tables S14 and S15, respectively. The experiment was conducted with a standard error of ±0.001 cm, and it was replicated three times under comparable conditions. Dimethylformamide (DMF) is employed as a negative control, while chloramphenicol serves as the positive standard for antibacterial activity.[16] Nystatin, on the other hand, is utilized as the positive standard for antifungal activity. The assessment of the activity involved measurement of the inhibition zone diameters of the ligand and metal complexes. Based on the findings obtained from the evaluation of the biology of integrin ligands and complexes with bacterial and fungal strains, it can be inferred. The results of the *in vitro* antibacterial and fungal activity tests indicated that the complexes exhibit a higher level of toxicity toward microorganisms compared to the ligand.[69] Furthermore, the present results were compared with the previous reports and are shown in Table S14. The results of this study clearly showed that CoL and CuL complexes had significant activity against *Aspergillus niger*. Additionally, the ZnL complex showed superior activity against *Rhizoctonia bataticola*. Furthermore, the biological activities of CoL, CuL, and ZnL complexes are found to be better than the previously reported standard biological agents against *Aspergillus flavus*.[70]

The absence of fungal growth in media containing the ligand and metal complexes, as indicated by the viability assay, served as well as evidence for the exceptional antibacterial properties of these compounds. The underlying principle entails the binding of the ligand and complexes to the surface of the cell membrane, thereby disrupting the cell's permeability and respiration mechanisms. The synthesized compounds exhibited the following order of biological activity: CuL > CoL > ZnL > H_2L. Moreover, it is probable that H_2L and CoL, CuL, and ZnL possess the capability to permeate the bacterial cells, in addition to their ability to bind to the surface of the cell membrane. The toxin cannot penetrate the bacterial cell wall and undergo reactions if its molecular shape and charge distribution are incompatible with the pores. Moreover, the present observed results were compared with the previous reports and are given in Table S15. The results of this study showed conclusively that the CoL and CuL complexes were effective against *Escherichia coli* and *Staphylococcus aureus*. Additionally, the ligand and CoL and CuL complexes exhibited outstanding activity against *Klebsiella pneumoniae*. The ligand, CuL, and ZnL complexes have exhibited improved effectiveness against *Proteus vulgaris* compared to previously studied compounds.[70] Overall, the results suggested that the studied metal complexes exhibited superior performance compared to the ligand when evaluated on the same microorganisms and under identical experimental conditions. The enhanced reactivity of the complexes arises from the formation of coordination bonds between the Schiff base and the metal ion. The chelation process decreases the polarity of the central metal ion.

4. CONCLUSIONS

A new ligand and three metal complexes have been synthesized, and they were characterized using analytical and spectral methods (FT-IR, UV−vis, NMR, and ESI-MS). According to elemental analysis, magnetic moments, and spectral data, all of the complexes have been confirmed to have a square planar geometry. DFT approaches were used to calculate the geometrical structures of the ligand and its metal complexes. The NBO analysis revealed that the natural charge of the metal ion, which was initially measured as +2.0e, decreased significantly during the complexation to +1.010e. This observation implies that electrons were transferred from the orbitals of the O and N atoms to the metal orbitals. The MEP analysis reveals that H_2L has pronounced negative regions near the O and N atoms, while the positive regions are mostly concentrated around the protons. The docking process involved H_2L and its metal complexes (CoL, CuL, and ZnL) interacting with the target protein HER2, which is linked to breast cancer. The findings support the CuL complex's potential as a new inhibitor of HER2 gene activity. Copper metal complexes exceed cobalt and zinc complexes in terms of antioxidant, antifungal, and antibacterial activities.

■ ASSOCIATED CONTENT

Supporting Information

The Supporting Information is available free of charge at https://pubs.acs.org/doi/10.1021/acsomega.3c08526.

Experimental analysis: electrochemical analysis and antioxidant activity; calculated UV and IR spectra for H_2L, CoL, CuL, and ZnL; ^1H NMR, ^{13}C NMR spectra, and ESI-HR mass spectra; *in vitro* antioxidant activity, antifungal activity, and antibacterial activity of the metal complexes and ligand; geometrical parameters; natural population analysis and natural electronic configuration; second order perturbation theory analysis results of the fock matrix; *in vitro* antioxidant (phosphomolybdenum method) activity of the metal complexes and Schiff base ligand; minimum inhibitory concentration values against the growth of fungi and bacteria (PDF)

■ AUTHOR INFORMATION

Corresponding Authors

Ganesan Venkatesh − *Department of Chemistry, Muthayammal Memorial College of Arts and Science, Namakkal, Tamil Nadu 637408, India*; orcid.org/0000-0002-0870-4542; Email: venkateshindhuja@gmail.com

Savas Kaya − *Department of Chemistry, Cumhuriyet University, Sivas 58140, Turkey*; orcid.org/0000-0002-0765-9751; Email: savaskaya@cumhuriyet.edu.tr

Authors

Palanisamy Vennila − *Department of Chemistry, Thiruvalluvar Government Arts College, Rasipuram, Tamil Nadu 637 401, India*

Samia Ben Ahmed − *Department of Chemistry, College of Sciences, King Khalid University, Abha 61413, Saudi Arabia*

Paramasivam Sumathi − *Department of Chemistry, Gobi Arts & Science College, Erode, Tamil Nadu 638452, India*

Vadivel Siva − *Department of Physics, Karpagam Academy of Higher Education, Coimbatore, Tamil Nadu 641021, India*

Premkumar Rajendran − *Department of Physics, N.M.S.S.V.N. College, Madurai, Tamil Nadu 625019, India*

https://doi.org/10.1021/acsomega.3c08526
ACS Omega 2024, 9, 8123−8138

Chennapan Kamal − *Department of Chemistry, Mahendra College of Engineering, Salem, Tamil Nadu 636106, India*

Complete contact information is available at: https://pubs.acs.org/10.1021/acsomega.3c08526

Notes

The authors declare no competing financial interest.

■ ACKNOWLEDGMENTS

The authors extend their appreciation to the Deanship of Scientific Research at King Khalid University, Saudi Arabia, for funding this work through Large Research Groups Program under grant number L.R.G.P2/3/44.

■ REFERENCES

(1) Aggoun, D.; Messasma, Z.; Bouzerafa, B.; Berenguer, R.; Morallon, E.; Ouennoughi, Y.; Ourari, A. Synthesis, characterization and DFT investigation of new metal complexes of Ni(II), Mn(II) and VO(IV) containing N,O-donor Schiff base ligand. *J. Mol. Struct.* **2021**, *1231*, No. 129923.

(2) Chen, L.; Wang, L.; An, W.; Wang, R.; Tian, L. Synthesis, structural characterization, and antibacterial activity of diorganotin complexes of Schiff base derived from 4- (diethylamino)-salicylaldehyde and L-tyrosine. *Inorg. Nano-Met. Chem.* **2020**, *50* (9), 872−879.

(3) Naureen, B.; Miana, G. A.; Shahid, K.; Asghar, M.; Tanveer, S.; Sarwar, A. Iron(III) and zinc(II) monodentate Schiff base metal complexes: synthesis, characterization and biological activities. *J. Mol. Struct.* **2021**, *1231*, No. 129946.

(4) Muthukkumar, M.; Kamal, C.; Venkatesh, G.; Kaya, C.; Kaya, S.; Enoch, I. V. M. V.; Vennila, P.; Rajavel, R. Structural, spectral, DFT and biological studies on macrocyclic mononuclear ruthenium (II) complexes. *J. Mol. Struct.* **2017**, *1147*, 502−514.

(5) Muthukkumar, M.; Rajavel, R.; Venkatesh, G.; Vennila, P. Macrocyclic Schiff Base Metal Complexes Derived from Isatin: Structural Activity Relationship and DFT Calculations. *Tenside Surfactants Detergents.* **2017**, *54*, 248−259.

(6) Kargar, H.; Ashfaq, M.; Fallah-Mehrjardi, M.; Behjatmanesh-Ardakani, R.; Munawar, K. S.; Tahir, M. N. Synthesis, crystal structure, spectral characterization, theoretical and computational studies of Ni(II), Cu(II) and Zn(II) complexes incorporating Schiff base ligand derived from 4-(diethylamino)salicylaldehyde. *Inorg. Chim. Acta* **2022**, *536*, No. 120878.

(7) Kumar, Y.; Singh, V. D.; Dwivedi, B. K.; Singh, N. K.; Pandey, D. S. Solid state emissive azo-Schiff base ligands and their Zn(ii) complexes: acidochromism and photoswitching behaviour. *New J. Chem.* **2021**, *45*, 199−207.

(8) Kargar, H.; Fallah-Mehrjardi, M.; Behjatmanesh-Ardakani, R.; Bahadori, M.; Moghadam, M.; Ashfaq, M.; Munawar, K. S.; Tahir, M. N. Synthesis, crystal structure, spectral characterization, catalytic studies and computational studies of Ni(II) and Pd(II) complexes of symmetrical tetradentate Schiff base ligand. *J. Coord. Chem.* **2022**, *75*, 972−993.

(9) Juyal, V. K.; Pathak, A.; Panwar, M.; Thakuri, S. C.; Prakash, Om; Agrwal, A.; Nand, V. Schiff base metal complexes as a versatile catalyst: a review. *J. Organomet. Chem.* **2023**, *999*, No. 122825.

(10) Radha, V. P.; Prabakaran, M. Novel thiadiazole-derived Schiff base ligand and its transition metal complexes, Thermal behaviour, theoretical study, chemo-sensor, antimicrobial, antidiabetic and anticancer activity. *Appl. Organomet. Chem.* **2022**, *36*, e6872.

(11) Mukherjee, D.; Reja, S.; Sarkar, K.; Fayaz, T. K. S.; Kumar, P.; Kejriwal, A.; Das, P.; Sanphui, P.; Das, R. K. In vitro cytotoxicity activity of copper complexes of imine and amine ligands: A combined experimental and computational study. *Inorg. Chem. Commun.* **2022**, *146*, No. 110190.

(12) Kaushik, S.; Paliwal, S. K.; Iyer, M. R.; Patil, V. M. Promising Schiff bases in antiviral drug design and discovery. *Med. Chem. Res.* **2023**, *32*, 1063−1076.

(13) Nair, M. S.; Arish, D.; Joseyphus, R. S. Synthesis, characterization, antifungal, antibacterial and DNA cleavage studies of some heterocyclic Schiff base metal complexes. *J. Saudi Chem. Soc.* **2012**, *16*, 83−88.

(14) Kumar, N.; Kaushal, R.; Awasthi, P. Non-covalent binding studies of transition metal complexes with DNA: A review. *J. Mol. Struct.* **2023**, *1288*, No. 135751.

(15) Boulechfar, C.; Ferkous, H.; Delimi, A.; Djedouani, A.; Kahlouche, A.; Boublia, A.; Darwish, A. S.; Lemaoui, T.; Verma, R.; Benguerba, Y. Schiff bases and their metal Complexes: A review on the history, synthesis, and applications. *Inorg. Chem. Commun.* **2023**, *150*, No. 110451.

(16) Yusuf, T. L.; Oladipo, S. D.; Zamisa, S.; Kumalo, H. M.; Lawal, I. A.; Lawal, M. M.; Mabuba, N. Design of new Schiff-Base Copper (II) complexes: Synthesis, crystal structures, DFT study, and binding potency toward cytochrome P450 3A4. *ACS Omega* **2021**, *6*, 13704−13718.

(17) Kumar, M.; Singh, A. K.; Singh, A. K.; Yadav, R. K.; Singh, S.; Singh, A. P.; Chauhan, A. Recent advances in 3d-block metal complexes with bi, tri, and tetradentate Schiff base ligands derived from salicylaldehyde and its derivatives: Synthesis, characterization and applications. *Coord. Chem. Rev.* **2023**, *488*, No. 215176.

(18) Singh, A.; Barman, P.; Gogoi, H. P. Thioether-based novel transition metal complexes: Synthesis, DNA interaction, in vitro biological assay, DFT calculations, and molecular docking studies. *Bioorg. Chem.* **2023**, *132*, No. 106343.

(19) Gull, P.; Hashmi, A. A. Synthesis, XRD and spectroscopic characterization of pharmacologically active Cu(II) and Zn(II) complexes. *J. Mol. Struct.* **2017**, *1139*, 264−268.

(20) Asath, R. M.; Premkumar, R.; Mathavan, T.; Benial, A. M. F. Spectroscopic and molecular docking studies on N,N-di-tert-butoxycarbonyl (Boc)-2-amino pyridine: A potential bioactive agent for lung cancer treatment. *J. Mol. Struct.* **2017**, *1143*, 415−423.

(21) Chohan, Z. H.; Munawar, A.; Supuran, C. T. Transition Metal Ion Complexes of Schiff-basesSynthesis, Characterization and Antibacterial Properties. *Met. Based Drugs* **2001**, *8*, 137−143.

(22) Ghosh, M. K.; Pathak, S.; Ghorai, T. K. Synthesis of Two Mononuclear Schiff Base Metal (M = Fe, Cu) Complexes: MOF Structure, Dye Degradation, H2O2 Sensing, and DNA Binding Property. *ACS Omega* **2019**, *4*, 16068−16079.

(23) Elemike, E. E.; Nwankwo, H. U.; Onwudiwe, D. C. Synthesis and comparative study on the anti-corrosion potentials of some Schiff base compounds bearing similar backbone. *J. Mol. Liq.* **2019**, *276*, 233−242.

(24) George, J.; Prasana, J. C.; Muthu, S.; Kuruvilla, T. K.; Sevanthi, S.; Saji, R. S. Spectroscopic (FT-IR, FT Raman) and quantum mechanical study on N-(2,6-dimethylphenyl)-2-{4-[2-hydroxy-3-(2-methoxyphenoxy)propyl]piperazin-1-yl}acetamide. *J. Mol. Struct.* **2018**, *1171*, 268−278.

(25) Muthu, S.; Ramachandran, G. Spectroscopic studies (FTIR, FT-Raman and UV−Visible), normal coordinate analysis, NBO analysis, first order hyper polarizability, HOMO and LUMO analysis of (1R)-N-(Prop-2-yn-1-yl)-2,3-dihydro-1H-inden-1-amine molecule by ab initio HF and density functional methods. *Spectrochimica Acta Part A: Molecular and Biomolecular Spectroscopy.* **2014**, *121*, 394−403.

(26) Porchelvi, E. E.; Muthu, S. Vibrational spectra, molecular structure, natural bond orbital, first order hyperpolarizability, thermodynamic analysis and normal coordinate analysis of Salicylaldehyde p-methylphenylthiosemicarbazone by density functional method. *Spectrochimica Acta Part A: Molecular and Biomolecular Spectroscopy.* **2015**, *134*, 453−464.

(27) Surendar, P.; Pooventhiran, T.; Al-Zaqri, N.; Rajam, S.; Rao, D. J.; Thomas, R. Synthesis of three quasi liquid Schiff bases between hexanal and adenine, cytosine, and l-leucine, structural interpretation, quantum mechanical studies and biological activity prediction. *J. Mol. Liq.* **2021**, *341*, No. 117305.

(28) Elangovan, N.; Thomas, R.; Sowrirajan, S. Synthesis of Schiff base (E)-4-((2-hydroxy-3,5-diiodobenzylidene)amino)-N-thiazole-2-yl)benzenesulfonamide with antimicrobial potential, structural features, experimental biological screening and quantum mechanical studies. *J. Mol. Struct.* **2022**, *1250*, No. 131762.
(29) Raja, G.; Venkatesh, G.; Al-Otaibi, J. S.; Vennila, P.; Mary, Y. S.; Sixto-López, Y. Synthesis, characterization, molecular docking and molecular dynamics simulations of benzamide derivatives as potential anti-ovarian cancer agents. *J. Mol. Struct.* **2022**, *1269*, No. 133785.
(30) Abbas, G.; Irfan, A.; Ahmed, I.; Al-Zeidaneen, F. K.; Muthu, S.; Fuhr, O.; Thomas, R. Synthesis and investigation of anti-COVID19 ability of ferrocene Schiff base derivatives by quantum chemical and molecular docking. *J. Mol. Struct.* **2022**, *1253*, No. 132242.
(31) Rajimon, K. J.; Elangovan, N.; Khairbek, A. A.; Thomas, R. Schiff bases from chlorine substituted anilines and salicylaldehyde: Synthesis, characterization, fluorescence, thermal features, biological studies and electronic structure investigations. *J. Mol. Liq.* **2023**, *370*, No. 121055.
(32) Geethapriya, J.; Devaraj, A. R.; Gayathri, K.; Swadhi, R.; Elangovan, N.; Manivel, S.; Sowrirajan, S.; Thomas, R. Solid state synthesis of a fluorescent Schiff base (E)-1-(perfluorophenyl)-N-(o-toly)methanimine followed by computational, quantum mechanical and molecular docking studies. *Results Chem.* **2023**, *5*, No. 100819.
(33) Ganesan, T. S.; Elangovan, N.; Vanmathi, V.; Sowrirajan, S.; Chandrasekar, S.; Murthy, K. R. S.; Thomas, R. Spectroscopic, Computational(DFT), Quantum mechanical studies and protein-ligand interaction of Schiff base 6,6-((1,2-phenylenebis-(azaneylylidene))bis(methaneylylidene))bis(2-methoxyphenol) from o-phenylenediamine and 3- methoxysalicylaldehyde. *Journal of the Indian Chemical Society.* **2022**, *99*, No. 100713.
(34) Paularokiadoss, F.; Jeyakumar, T. C.; Thomas, R.; Sekar, A.; Bhakiaraj, D. Group 13 monohalides [AX (A = B, Al, Ga and In; X = Halogens)] as alternative ligands for carbonyl in organometallics: Electronic structure and bonding analysis. *Comput. Theor. Chem.* **2022**, *1209*, No. 113587.
(35) Mani, N.; Nicksonsebastin, D.; Prasath, M.; Mishma, J. N. C.; Kadaikunnan, S.; Abbas, G.; Muthu, S. Potential energy surface, effect of solvents in molecular level, experimental spectra (FTIR, Raman, UV−visible & NMR), electronic, and dynamics simulation of isobavachalcone − Anti tuberculosis agent. *J. Mol. Liq.* **2023**, *392*, No. 123465.
(36) Vedhapriya, K.; Balaji, G.; Dhiyaneshwari, B.; Kumaran, S.; Narayana, B.; Kodlady, S. N.; Kadaikunnan, S.; Abbas, G.; Muthu, S. Synthesis, molecular structure, experimental and theoretical characterization of 3-((2-(2,4-dinitrophenyl) hydrazone) methyl) pyridine-Carcinopreventive activity (in silico and in vitro investigation). *J. Mol. Struct.* **2023**, *1294*, No. 136527.
(37) Frisch, M. J.; Trucks, G. W.; Schlegel, H. B.; Scuseria, G. E.; Robb, M. A.; Cheeseman, J. R.; Montgomery, Jr., J. A.; Vreven, T.; Kudin, K. N.; Burant, J. C.; Millam, J. M.; Iyengar, S. S.; Tomasi, J.; Barone, V.; Mennucci, B.; Cossi, M.; Scalmani, G.; Rega, N.; Petersson, G. A.; Nakatsuji, H.; Hada, M.; Ehara, M.; Toyota, K.; Fukuda, R.; Asegawa, J.; Ishida, M.; Nakajima, T.; Honda, Y.; Kitao, O.; Nakai, H.; Klene, M.; Knox, X.; Li, J. E.; Hratchian, H. P.; Cross, J. B.; Adamo, C.; Jaramillo, J.; Gomperts, R.; Stratmann, R. E.; Yazyev, O.; Austin, A. J.; Cammi, R.; Pomelli, C.; Ochterski, J. W.; Ayala, P. Y.; Morokuma, K.; Voth, G. A.; Salvador, P.; Dannenberg, J. J.; Zakrzewski, V. G.; Dapprich, S.; Daniels, A. D.; Strain, M. C.; Farkas, O.; Malick, D. K.; Rabuck, A. D.; Raghavachari, K.; Foresman, J. B.; Ortiz, J. V.; Cui, Q.; Baboul, A. G.; Clifford, S.; Ioslowski, J.; Stefanov, B. B.; Liu, G.; Liashenko, A.; Piskorz, P.; Komaromi, I.; Martin, R. L.; Fox, D. J.; Keith, T.; AlLaham, M. A.; Peng, C. Y.; Nanayakkara, A.; Challacombe, M.; Gill, P. M. W.; Johnson, B.; Chen, W.; Wong, M. W.; Gonzalez, C.; Pople, J. A. *Gaussian 03, Revision E.01*; Gaussian Inc,. Pittsburgh. B.A. 2000: Walliford CT. 2009, 121, 150.
(38) Jamróz, M. H. Vibrational Energy Distribution Analysis VEDA 4, *Warsaw*, 2004.
(39) Morris, G. M.; Goodsell, D. S.; Halliday, R. S.; Huey, R.; Hart, W. E.; Belew, R. K.; Olson, A. J. Automated docking using a Lamarckian genetic algorithm and an empirical binding free energy function. *J. Comput. Chem.* **1998**, *19*, 1639.
(40) *The PyMOL Molecular Graphics System*, Version 1.7.4.5 Schrödinger, LLC. http://www.rcsb.org/pdb.
(41) http://www.rcsb.org/pdb.
(42) Akram, N.; Mansha, A.; Premkumar, R.; Benial, A. M. F.; Usman, M.; Rasool, N.; Asim, S. Spectroscopic, quantum chemical and molecular docking studies of 2-Hydroxy-4′-(2-hydroxyethoxy)-2-methylpropiophenone: A potent anti-Alzheimer's drug. *Chem. Data Collect.* **2020**, *29*, No. 100495.
(43) Ali, O. A. A.; Elangovan, N.; Mahmoud, S. F.; El-Gendey, M. S.; Elbasheer, H. Z. E.; El-Bahy, S. M.; Thomas, R. Synthesis, characterization, vibrational analysis and computational studies of a new Schiff base from pentafluoro benzaldehyde and sulfanilamide. *J. Mol. Struct.* **2022**, *1265*, No. 133445.
(44) Roby, O.; Kadiri, F. Z.; Loukhmi, Z.; Moutaouakil, M.; Tighadouini, S.; Saddik, R.; Aboulmouhajir, A. Synthesis of new set of imidazo[1,2-a]pyridine-schiff bases derivatives as potential antimicrobial agents: Experimental and theoretical approaches. *J. Mol. Struct.* **2023**, *1292*, No. 136186.
(45) Adly, O. M. I.; Shebl, M.; Abdelrhman, E. M.; El-Shetary, B. A. Synthesis, spectroscopic, X-ray diffraction, antimicrobial and anti-tumor studies of Ni(II) and Co(II) complexes derived from 4-acetyl-5,6-diphenyl-3(2H)-pyridazinone and ethylenediamine. *J. Mol. Struct.* **2020**, *1219*, No. 128607.
(46) Aravindan, P.; Sivaraj, K.; Kamal, C.; Vennila, P.; Venkatesh, G. Synthesis, Molecular structure, Spectral Characterization, Molecular docking and biological activities of (E)-N-(2-methoxy benzylidene) anthracene-2-amine and Co(II), Cu(II) and Zn(II) complexes. *J. Mol. Struct.* **2021**, *1229*, No. 129488.
(47) Vennila, P.; Venkatesh, G.; Sixto-López, Y.; Kamal, C.; Kaya, S.; Serdaroğlu, G.; Landeros-Rivera, B. Synthesis, spectroscopic characterization, molecular docking studies and DFT calculation of novel Mannich base 1-((4-ethylpiperazin-1-yl)(2-hydroxyphenyl)methyl)-naphthalen-2-ol. *J. Mol. Struct.* **2021**, *1246*, No. 131164.
(48) Vennila, P.; Al-Otaibi, J. S.; Venkatesh, G.; Mary, Y. S.; Raj, V.; Acharjee, N.; Tamilselvi, P. Structural, Spectral, Molecular Docking, and Molecular Dynamics Simulations of Phenylthiophene-2-Carboxylate Compounds as Potential Anticancer Agents. *Polycyclic Aromat. Compd.* **2024**, *44*, 238.
(49) Kusmariya, B. S.; Tiwari, S.; Tiwari, A.; Mishra, A. P.; Naikoo, G. A.; Pandit, U. J. Theoretical and experimental studies of two Co(II) and Ni(II) coordination complex with N,O donor 2-chloro-6-{[(4-hydroxy-3-methoxyphenyl)methylidene]amino}-4 nitrophenol ligand. *J. Mol. Struct.* **2016**, *1116*, 279−291.
(50) Venkatesh, G.; Sixto-López, Y.; Vennila, P.; Mary, Y. S.; Correa-Basurto, J.; Mary, Y. S.; Manikandan, A. An investigation on the molecular structure, interaction with metal clusters, anti-Covid-19 ability of 2-deoxy-D-glucose: DFT calculations, MD and docking simulations. *J. Mol. Struct.* **2022**, *1258*, No. 132678.
(51) Halim, S. A.; Shebl, M. Synthesis, spectral, structural, DFT and NLO studies of cerium(III) and thorium(IV) complexes of 1-(5-(1-(2-aminophenylimino)ethyl)-2,4-dihydroxyphenyl)ethanone. *J. Coord. Chem.* **2021**, *74*, 2984−3001.
(52) Shebl, M. Mononuclear, homo- and hetero-binuclear complexes of 1-(5-(1-(2-aminophenylimino)ethyl)-2,4-dihydroxyphenyl)-ethanone: synthesis, magnetic, spectral, antimicrobial, antioxidant, and antitumor studies. *J. Coord. Chem.* **2016**, *69*, 199−214.
(53) Sakthivel, R. V.; Sankudevan, P.; Vennila, P.; Venkatesh, G.; Kaya, S.; Serdaroğlu, G. Experimental and theoretical analysis of molecular structure, vibrational spectra and biological properties of the new Co(II), Ni(II) and Cu(II) Schiff base metal complexes. *J. Mol. Struct.* **2021**, *1233*, No. 130097.
(54) Mamun, M. A.; Ahmed, O.; Bakshi, P. K.; Ehsan, M. Q. Synthesis and spectroscopic, magnetic and cyclic voltammetric characterization of some metal complexes of methionine: [(C5H10NO2S)2MII]; MII = Mn(II), Co(II), Ni(II), Cu(II), Zn(II), Cd(II) and Hg(II). *J. Saudi Chem. Soc.* **2010**, *14*, 23−31.

https://doi.org/10.1021/acsomega.3c08526
ACS Omega 2024, 9, 8123−8138

(55) El-Hamid, S. M. A.; Sadeek, S. A.; Sadek, N. B.; Sabry, M. A.; El-Gedamy, M. S. Novel nano-sized metal complexes based on aceclofenac and glycine ligands: Synthesis, Characterization, molecular docking studies and their enhanced efficacy in ameliorating testicular and spermatological oxidative damages in male rats. *J. Mol. Liq.* **2023**, *391*, No. 123274.
(56) El-Hamid, S. M. A.; Sadeek, S. A.; Mohammed, S. F.; Ahmed, F. M.; El-Gedamy, M. S. N_2O_2-chelate metal complexes with Schiff base ligand: Synthesis, characterisation and contribution as a promising antiviral agent against human cytomegalovirus. *Appl. Organomet. Chem.* **2023**, *37*, e6958.
(57) Venkatesh, G.; Haseena, S.; Al-Otaibi, J. S.; Mary, Y. S.; Vennila, P.; Mary, Y. S.; Azad, S. A. Observations into the reactivity, docking, DFT, and MD simulations of fludarabine and clofarabine in various solvents. *J. Mol. Liq.* **2023**, *383*, No. 122076.
(58) Weinhold, F.; Landis, C. R.; Glendening, E. D. What is NBO analysis and how is it useful? *Int. Rev. in Phys. Chem.* **2016**, *35* (3), 399−440.
(59) Islam, N.; Kaya, S.; (Eds.). *Conceptual Density Functional Theory and Its Application in the Chemical Domain*. CRC Press. 2018.
(60) Venkatesh, G.; Govindaraju, M.; Kamal, C.; Vennila, P.; Kaya, S. Structural, electronic and optical properties of 2,5-dichloro-*p*-xylene: experimental and theoretical calculations using DFT method. *RSC Adv.* **2017**, *7*, 1401−1412.
(61) Parr, R. G.; Szentpaly, L. V.; Liu, S. Electrophilicity Index. *J. Am. Chem. Soc.* **1999**, *121*, 1922−1924.
(62) Koopmans, T. Über die Zuordnung von Wellenfunktionen und Eigenwerten zu den Einzelnen Elektronen Eines Atoms. *Physica* **1934**, *1*, 104−113.
(63) Parr, R. G.; Pearson, R. G. Absolute hardness: companion parameter to absolute electronegativity. *J. Am. Chem. Soc.* **1983**, *105*, 7512−7516.
(64) Kanagavalli, A.; Jayachitra, R.; Thilagavathi, G.; Padmavathy, M.; Elangovan, N.; Sowrirajan, S.; Thomas, R. Synthesis, structural, spectral, computational, docking and biological activities of Schiff base (E)-4-bromo-2-hydroxybenzylidene) amino)-N-(pyrimidin-2-yl) benzenesulfonamide from 5-bromosalicylaldehyde and sulfadiazine. *Journal of the Indian Chemical Society.* **2023**, *100*, No. 100823.
(65) Prihantono; Irfandi, R.; Raya, I.; Warsinggih. Potential anticancer activity of Mn (II) complexes containing arginine dithiocarbamate ligand on MCF-7 breast cancer cell lines. *Ann. Med. Surg.* **2020**, *60*, 396−402.
(66) Mohamed, G. G.; Mahmoud, W. H.; Refaat, A. M.; Gao, N. Nano-Azo Ligand and Its Superhydrophobic Complexes: Synthesis, Characterization, DFT, Contact Angle, Molecular Docking, and Antimicrobial Studies. *J. Chem.* **2020**, *2020*, 6382037.
(67) Rodríguez-Arce, E.; Saldías, M. Antioxidant properties of flavonoid metal complexes and their potential inclusion in the development of novel strategies for the treatment against neurodegenerative diseases. *Biomedicine & Pharmacotherapy* **2021**, *143*, No. 112236.
(68) Hasan, M. M.; Ahsan, H. M.; Saha, P.; Naime, J.; Das, A. K.; Asraf, M. A.; Islam, A. B. M. N. Antioxidant, antibacterial and electrochemical activity of (E)-N-(4 (dimethylamino) benzylidene)-4H-1,2,4-triazol-4-amine ligand and its transition metal complexes. *Results Chem.* **2021**, *3*, No. 100115.
(69) El-ghamry, M. A.; Elzawawi, F. M.; Aziz, A. A. A.; Nassir, K. M.; Abu-El-Wafa, S. M. New Schiff base ligand and its novel Cr(III), Mn(II), Co(II), Ni(II), Cu(II), Zn(II) complexes: spectral investigation, biological applications, and semiconducting properties. *Sci. Rep* **2022**, *12*, 17942.
(70) Nair, M. S.; Arish, D.; Joseyphus, R. S. Synthesis, characterization, antifungal, antibacterial and DNA cleavage studies of some heterocyclic Schiff base metal complexes. *J. Saudi Chem. Soc.* **2012**, *16*, 83−88.

https://doi.org/10.1021/acsomega.3c08526
ACS Omega 2024, 9, 8123−8138